

# Ultrasound-array-based real-time photoacoustic microscopy of human pulsatile dynamics *in vivo*

**Liang Song**

**Konstantin Maslov**

Washington University in St. Louis  
Department of Biomedical Engineering  
Optical Imaging Laboratory  
One Brookings Drive  
St. Louis, Missouri 63130

**K. Kirk Shung**

University of Southern California  
Department of Biomedical Engineering  
1042 Downey Way  
Los Angeles, California 90089

**Lihong V. Wang**

Washington University in St. Louis  
Department of Biomedical Engineering  
Optical Imaging Laboratory  
One Brookings Drive  
St. Louis, Missouri 63130

**Abstract.** With a refined ultrasound-array-based real-time photoacoustic microscopy (UA-PAM) system, we demonstrate the feasibility of noninvasive *in vivo* imaging of human pulsatile dynamics. The system, capable of real-time B-scan imaging at 50 Hz and high-speed 3-D imaging, is validated by imaging the subcutaneous microvasculature in rats and humans. After the validation, a human artery around the palm-wrist area is imaged, and its pulsatile dynamics, including the arterial pulsatile motion and changes in hemoglobin concentration, is monitored with 20-ms B-scan imaging temporal resolution. To our knowledge, this is the first demonstration of real-time photoacoustic imaging of human physiological dynamics. Our results show that UA-PAM can potentially enable many new possibilities for studying functional and physiological dynamics in both preclinical and clinical imaging settings. © 2010 Society of Photo-Optical Instrumentation Engineers. [DOI: 10.1117/1.3333545]

**Keywords:** imaging systems; photoacoustics; ultrasonics; optical systems; optics.

Paper 092845SR received Jul. 8, 2009; revised manuscript received Sep. 15, 2009; accepted for publication Sep. 22, 2009; published online Mar. 11, 2010.

## 1 Introduction

Due to the requirement for both high imaging speed and non-invasiveness, it remains challenging to precisely image and quantify human physiological dynamics *in vivo* in real time. Magnetic resonance imaging (MRI) provides good functional imaging capability, but it usually cannot perform real-time imaging.<sup>1</sup> Ultrasound offers real-time imaging capability, but the mechanical contrast does not provide much physiological information besides flow.<sup>2</sup> Previously available high-resolution optical microscopy modalities—including confocal microscopy,<sup>3</sup> two-photon microscopy,<sup>4</sup> and optical coherence tomography<sup>5</sup>—are capable of real-time imaging. However, as none of them sense optical absorption directly, contrast agents are usually required for physiological imaging. Moreover, they rely on the detection of ballistic photons, and thus cannot image beyond one optical transport mean free path in highly scattering biological tissue ( $\sim 1$  mm).

Photoacoustic tomography is a recently developed, noninvasive biomedical imaging technology that provides excellent optical absorption contrast—endogenous contrast for many physiological phenomena—with high ultrasonic resolution at superdepths—depths beyond the optical transport mean free path.<sup>6</sup> It has been used to study whisker stimulation,<sup>7</sup> single vessel oxygenation,<sup>8</sup> and tumor hypoxia.<sup>9</sup> Photoacoustic tomography is also a high-speed imaging modality by nature, with its speed fundamentally limited by the photoacoustic wave propagation time. In principle, A-lines (i.e., depth resolved 1-D images) can be acquired at a rate of up to 100 kHz at a depth of 1.5 cm. With a 30-MHz ultrasound array and a

kilohertz repetition laser system, we have developed a photoacoustic microscopy imaging system that performs real-time B-scan imaging at 50 Hz and high-speed 3-D imaging, offering the feasibility of imaging physiological dynamics.<sup>10–12</sup> In addition, this ultrasound-array-based photoacoustic microscopy (UA-PAM) system, with axial, lateral, and elevational resolutions of 25, 70, and 200  $\mu\text{m}$ , respectively, provides  $\sim 3$ -mm imaging depth in scattering biological tissue.<sup>10</sup>

In this paper, with system refinement, we report significant improvement in the image quality of UA-PAM, which enabled the imaging of microvasculature details in rats and humans. In addition, the 20-ms B-scan imaging temporal resolution offered the capability to noninvasively monitor human pulsatile dynamics—including arterial pulsatile motion and changes in hemoglobin concentration—*in vivo*. To our knowledge, this is the first demonstration of real-time photoacoustic imaging of human physiological dynamics.

## 2 Methods and Materials

The system configuration is shown in Fig. 1. The details of the system can be found in our previous publications.<sup>10–12</sup> In this paper, to excite photoacoustic waves, we used light at 570 nm, which corresponds to an isosbestic point where oxy- and deoxyhemoglobin molecules have the same molar optical absorption coefficient.

To couple the generated photoacoustic waves to the ultrasound-array transducer, we used a water container (filled with deionized water) with a window of low-density polyethylene (LDPE) film, to substitute for the water-filled transparent plastic piece in our previous system.<sup>10</sup> As a result, the skin surface was not directly contacted by the scanning probe dur-

Address all correspondence to: Lihong V. Wang, Washington University in St. Louis, Department of Biomedical Engineering, Optical Imaging Laboratory, One Brookings Drive, St. Louis, Missouri 63130. Tel: 314-935-6152; Fax: 314-935-7448; E-mail: lhwwang@biomed.wustl.edu

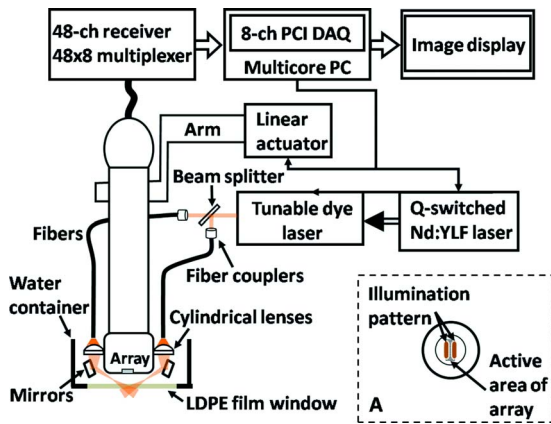


**Fig. 1** Schematic of the refined UA-PAM system. Inset A, optical illumination pattern on the skin surface.

ing the experiments, and disturbance to the imaged object was minimized. As before, acoustic gel was used to improve the ultrasonic coupling between the skin surface and the LDPE film. Compared with the previous system, the chances for air-bubble generation in the gel during the mechanical scanning (for 3-D imaging) of the probe were significantly reduced, as both the skin and the film were static. Furthermore, the number of optical interfaces was reduced, which increased the light delivery efficiency. Fine-tuning of the light delivery was performed<sup>10</sup> to optimize the system's SNR. All animal and human experiments described here were carried out in compliance with Washington University approved protocols.

To validate the refined UA-PAM system, Sprague Dawley rats (Harlan Laboratories, Inc., Indianapolis, Indiana) were imaged. Intradermal injection of a mixture of ketamine (85 mg/kg) and xylazine (15 mg/kg) was used for anesthesia. Before photoacoustic imaging, the hair in the imaged region was removed with commercial depilatory lotion.

The UA-PAM system is also safe for human use. For human imaging, the optical fluence on the skin surface was set to  $\sim 0.5$  mJ/cm<sup>2</sup> per pulse, well below the ANSI<sup>13</sup> recommended maximum permissible exposure (MPE) of 20 mJ/cm<sup>2</sup> for a single pulse in the visible spectral range. For 10 s of continuous real-time B-scan imaging (at 50 Hz), 3000 laser pulses were delivered to the skin surface, corresponding to a time-averaged light intensity of  $\sim 150$  mW/cm<sup>2</sup>, below the ANSI recommended MPE of 196 mW/cm<sup>2</sup>, calculated by  $1.1t^{0.25}$  W/cm<sup>2</sup>. For 3-D imaging, the laser pulse repetition rate was increased to 996 Hz. However, in this case, the total illuminated area was also increased due to the mechanical scanning of the probe, resulting in a time-averaged light intensity of  $\sim 300$  mW/cm<sup>2</sup>, below the 1.1 W/cm<sup>2</sup> ANSI safety standard based on the same calculation.

### 3 Results

An *in vivo* photoacoustic maximum amplitude projection (MAP) image—the maximum photoacoustic amplitudes projected along the depth direction to the skin surface—of a rat [Fig. 2(a)] weighing  $\sim 280$  g is shown in Fig. 2(b). Compared with previous results,<sup>10</sup> more microvasculature details were imaged with the refined UA-PAM system. Figure 2(c) is a

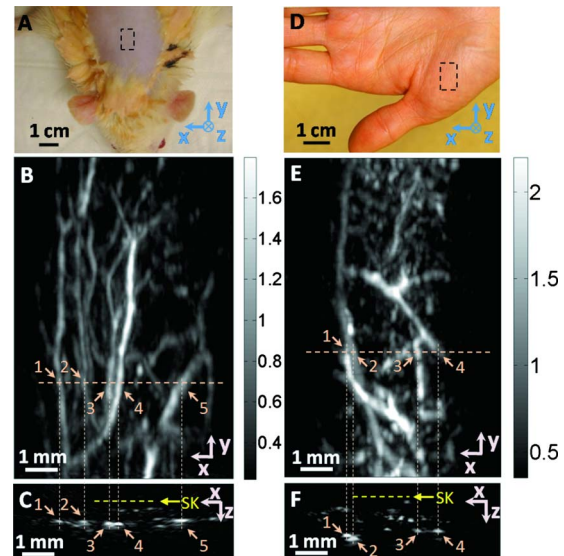
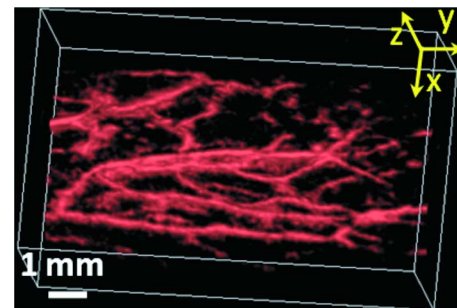


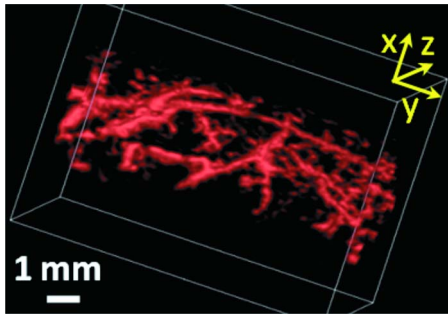
**Fig. 2** Noninvasive *in vivo* photoacoustic images acquired by the refined UA-PAM system. (a) Photograph of a Sprague Dawley rat with hair removed before photoacoustic imaging, where  $x$  represents the beamforming (B-scan) direction,  $y$  represents the mechanical scanning direction, and  $z$  represents the depth direction. The dashed rectangle indicates the imaged area. (b) Photoacoustic MAP image of the rat. The gray-scale represents relative optical absorption. (c) Photoacoustic B-scan image corresponding to the dashed horizontal line in (b), showing the depths of the blood vessels: SK, skin surface. Numbers 1 to 5 indicate corresponding blood vessels in (b) and (c). (d) Photograph of a human hand. The dashed rectangle indicates the imaged area. (e) Photoacoustic MAP image of the hand. (f) Photoacoustic B-scan image corresponding to the dashed horizontal line in (e). Numbers 1 to 4 indicate corresponding blood vessels in (e) and (f).

B-scan image corresponding to the dashed line in Fig. 2(b), showing subcutaneous blood vessels at various depths up to 1 mm below the rat's skin surface. The imaged blood vessels are of diameters of  $\sim 70$  to  $300$   $\mu$ m. To view the vasculature from different perspectives, a 3-D animation (Video 1), showing blood vessels in different layers, was constructed with VolView (Kitware, Clifton Park, New York). More features, including rotation, scaling, and zooming, are available with the software.

To demonstrate the feasibility of human imaging with UA-PAM, we imaged the palm of a human hand [Fig. 2(d)]. The subcutaneous microvasculature of the hand was imaged with a



**Video 1** Photoacoustic 3-D animation of the rat (QuickTime, 4.05 MB). [URL: <http://dx.doi.org/10.1117/1.3333545.1>].



**Video 2** Photoacoustic 3-D animation of the human hand (QuickTime, 4.50 MB). [URL: <http://dx.doi.org/10.1117/1.3333545.2>].

quality comparable to that of the aforementioned rat images. The imaged blood vessels in the human hand are larger though, ranging from  $\sim 100$  to  $400\ \mu\text{m}$  [Fig. 2(e)]. The depths of the blood vessels were clearly shown in the B-scan image [Fig. 2(f)]. Subcutaneous blood vessels up to 1.2 mm deep were imaged in this case. Due to the overlap, some relatively small blood vessels are not well shown in the MAP image. However, these vessels, along with the layered vascular structures, are clearly seen in the 3-D animation (Video 2).

To study the pulsatile dynamics, we scanned a region of the palm near the wrist, where an apparent artery,  $\sim 1$  mm in diameter and over 1 mm deep, was imaged [Fig. 3(a)]. After acquiring the initial 3-D image, we fixed the scanning probe to perform 10-s real-time B-scan imaging across the artery [Fig. 3(b) and Video 3]. Due to the strong optical absorption of hemoglobin at 570 nm (absorption coefficient  $\mu_a \approx 200\ \text{cm}^{-1}$ ), the bottom part of the artery was not well imaged. But the motion dynamics of the arterial pulsation was clearly captured. An M-mode image across the center of the artery, showing the details of the pulsatile motion, is shown in Fig. 3(c). The pulsatile rate, estimated from the image, was 66/min, consistent with the  $65 \pm 2/\text{min}$  rate measured from a pulse oximeter. For comparison, an M-mode image of a vein was plotted in Fig. 3(d), from which weak motion of the vein was revealed. Presumably, the motion was due to artery-pulsation-induced skin movement (observable in Video 3). As seen from Fig. 3(d), the vein's motion was indeed weakly correlated with the artery pulsation. However, compared with the artery [Fig. 3(c)], the vein's motion was much weaker.

To supplement tissue structural information, and to validate the observed artery motion, we acquired ultrasound images of similar regions using a commercial ultrasound machine (iU22 with a L15-7io Compact Linear Array, Philips Healthcare, Andover, Massachusetts). The ultrasound transducer, covering frequencies  $\sim 7$  to 15 MHz, provides sufficient resolution to resolve the artery that was photoacoustically imaged. In the ultrasound images, it was interesting to see that the artery only expanded apparently in the direction normal to the skin surface (Video 4). In the direction parallel to the skin surface, the expansion was almost negligible. This type of motion was likely due to the anisotropy of the surrounding tissue structure, namely, the surrounding tissue can be more easily stretched perpendicularly to the skin surface than parallelly to the skin surface. The observed motion in the ultrasound images was consistent with the result seen in real-time photoacoustic imaging, where apparent motion was ob-

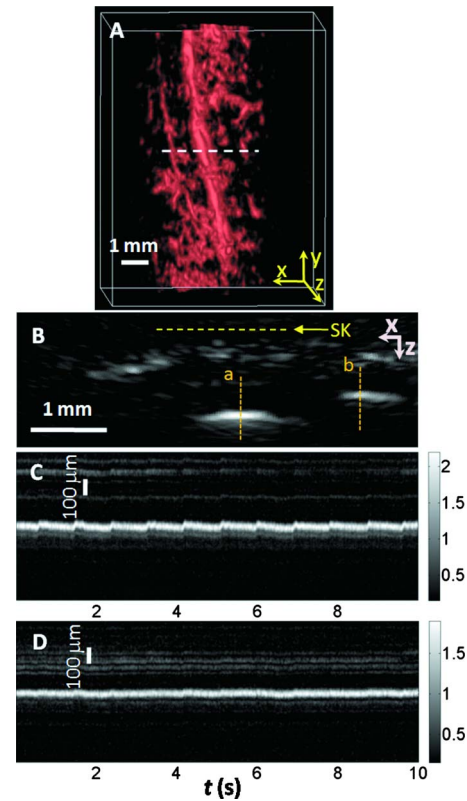
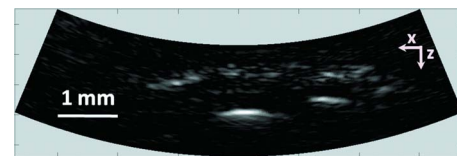


**Fig. 3** Dynamic noninvasive *in vivo* photoacoustic imaging by the refined UA-PAM system: (a) *In vivo* 3-D photoacoustic image of a human hand, the dashed line indicates the cross section monitored by real-time B-scan imaging; (b) one B-scan image corresponding to the dashed horizontal line in (a), SK, skin surface; (c) M-mode image corresponding to the dotted vertical line a in (b), showing the arterial pulsatile motion as a function of time; and (d) M-mode image of a vein corresponding to the dotted vertical line b in (b).

served only in the skin's normal direction. In addition, the M-mode images acquired with our UA-PAM system agreed well with those acquired by the commercial ultrasound machine, which, however, did not show as much fine details as the UA-PAM system did.

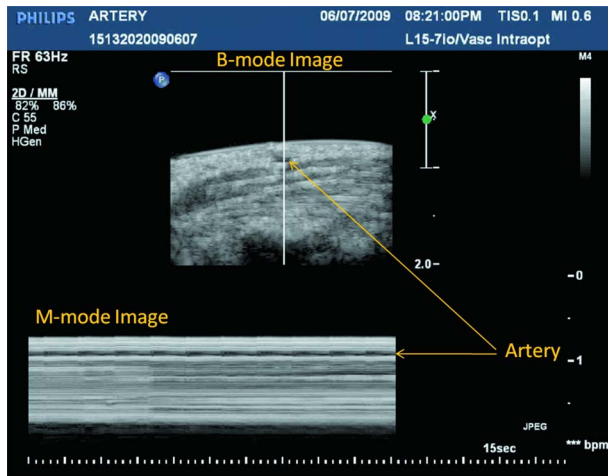
#### 4 Discussion and Conclusions

One drawback of ultrasound imaging is that little physiological information besides flow can be provided. By contrast, photoacoustic imaging has the potential to offer both hemoglobin concentration and oxygen saturation information. Ideally, to better characterize the pulsatile hemodynamics, oxygen saturation should be measured within each cardiac cycle.



**Video 3** Real-time photoacoustic B-scan imaging of the arterial pulsation (QuickTime, 690 KB). [URL: <http://dx.doi.org/10.1117/1.3333545.3>].





**Video 4** Ultrasound images of the arterial pulsation. The upper panel shows B-mode images, while the bottom one shows M-mode images corresponding to the vertical line in the upper panel (QuickTime, 2.84 MB). [URL: <http://dx.doi.org/10.1117/1.3333545.4>].

However, accurate computation of the blood oxygenation in real-time requires photoacoustic imaging with laser-wavelength tunability in real time (because oxygenation quantification requires multiwavelength measurements), which is currently not available in our laser system. Fortunately, the change in hemoglobin concentration can be monitored already with UA-PAM. Although the arterial pulsatile motions were apparent [Fig. 3(c) and Video 3], we found that the hemoglobin concentration was approximately constant with time—the standard deviation of the signal normalized by the temporal maximum value was 0.02. We also studied the hemoglobin concentration dynamics of a vein, which showed similar results. This observation agreed with the fact that, under normal physiological conditions, the hemoglobin concentration does not change significantly.

A few factors—including hemoglobin concentration, oxygenation, and vessel diameter and position—can potentially affect the magnitude (instead of position) of the received photoacoustic signal; in general, they may not be decoupled easily. In this study, however, we believe that any observable change in the magnitude of the signal, if any, would be due primarily to the hemoglobin concentration variation. Conversely, the lack of such change in the observable signal suggests that the hemoglobin concentration was approximately constant. Our reasoning is as follows.

1. The 570-nm wavelength that we used corresponds to an isosbestic point; therefore, oxygenation does not affect the photoacoustic signal.

2. In principle, without considering the limited acoustic receiving aperture and reconstruction imperfection, the signal should be proportional to the square root of the vessel diameter.<sup>6</sup> With a blood-vessel-mimicking phantom of  $\sim 1$  mm diameter, we found that a 15% diameter variation would induce only  $\sim 2\%$  signal change, smaller than the theoretical value. Given the  $\sim 2\%$  noise level (without averaging), only greater diameter variations can generate observable signal changes. In addition, the vasodilation was apparent only in the depth direction, further reducing the dilation-induced signal change, and making it essentially negligible.

3. Experiments with phantoms also showed that, around the acoustic elevational focus, a  $50\text{-}\mu\text{m}$  displacement in the depth direction would induce only a  $\sim 1.5\%$  signal change. In fact, during our experiment, we did not observe any significant change of the artery position. Even if we took into account the vasodilation-induced displacement ( $\sim 50\text{ }\mu\text{m}$ ), the signal change would still be negligible.

In summary, our refined UA-PAM system performed high-speed *in vivo* imaging of microvasculature details in both rats and humans with improved quality. With this UA-PAM system, hemoglobin concentration dynamics and arterial pulsatile motion were captured in real time, for the first time to our knowledge. With the promising results shown in this study, we believe that UA-PAM will open up many new possibilities for studying functional and physiological dynamics in both preclinical and clinical imaging settings.

### Acknowledgments

This work was sponsored in part by National Institutes of Health Grants U54 CA136398 (NTR), R01 EB000712, R01 NS46214 (BRP), and R01 EB008085. L.W. has a financial interest in Microphotoacoustics, Inc., and Endra, Inc., which, however, did not support this work. The authors are grateful to Christopher Favazza, Chulhong Kim, Joon-Mo Yang, Song Hu, and Todd Erpelding for beneficial discussions. They also thank Professor Jim Ballard for careful proofreading.

### References

1. R. M. Heidemann, O. Ozsarlak, P. M. Parizel, J. Michiels, B. Kiefer, V. Jellus, M. Muller, F. Breuer, M. Blaimer, M. A. Griswold, and P. M. Jakob, "A brief review of parallel magnetic resonance imaging," *Eur. Radiol.* **13**(10), 2323–2337 (2003).
2. P. N. T. Wells, "Ultrasound imaging," *Phys. Med. Biol.* **51**(13), R83–R98 (2006).
3. R. H. Webb, "Confocal optical microscopy," *Rep. Prog. Phys.* **59**(3), 427–471 (1996).
4. W. Denk, J. H. Strickler, and W. W. Webb, "Two-photon laser scanning fluorescence microscopy," *Science* **248**(4951), 73–76 (1990).
5. D. Huang, E. A. Swanson, C. P. Lin, J. S. Schuman, W. G. Stinson, W. Chang, M. R. Hee, T. Flotte, K. Gregory, C. A. Puliafito, and J. G. Fujimoto, "optical coherence tomography," *Science* **254**(5035), 1178–1181 (1996).
6. M. H. Xu and L. H. V. Wang, "Photoacoustic imaging in biomedicine," *Rev. Sci. Instrum.* **77**(4), 041101 (2006).
7. X. D. Wang, Y. J. Pang, G. Ku, X. Y. Xie, G. Stoica, and L. H. V. Wang, "Noninvasive laser-induced photoacoustic tomography for structural and functional *in vivo* imaging of the brain," *Nat. Biotechnol.* **21**(7), 803–806 (2003).
8. H. F. Zhang, K. Maslov, G. Stoica, and L. H. V. Wang, "Functional photoacoustic microscopy for high-resolution and noninvasive *in vivo* imaging," *Nat. Biotechnol.* **24**(7), 848–851 (2006).
9. M. L. Li, J. T. Oh, X. Y. Xie, G. Ku, W. Wang, C. Li, G. Lungu, G. Stoica, and L. V. Wang, "Simultaneous molecular and hypoxia imaging of brain tumors *in vivo* using spectroscopic photoacoustic tomography," *Proc IEEE* **96**(3), 481–489 (2008).
10. L. Song, K. Maslov, R. Bitton, K. K. Shung, and L. V. Wang, "Fast 3-D dark-field reflection-mode photoacoustic microscopy *in vivo* with a 30-MHz ultrasound linear array," *J. Biomed. Opt.* **13**(5), 054028 (2008).
11. R. J. Zemp, L. Song, R. Bitton, K. K. Shung, and L. V. Wang, "Real-time photoacoustic microscopy *in vivo* with a 30-MHz ultrasound array transducer," *Opt. Express* **16**(11), 7915–7928 (2008).
12. R. J. Zemp, L. Song, R. Bitton, K. K. Shung, and L. V. Wang, "Real-time photoacoustic microscopy of murine cardiovascular dynamics," *Opt. Express* **16**(22), 18551–18556 (2008).
13. The Laser Institute of America, *American National Standard for Safe Use of Lasers (ANSI Z136.1-2000)*, The Laser Institute of America, Orlando, FL (2000).